Review of the Development of Diamond Radiation Sensors

The RD42 Collaboration

W. Adam[1], C. Bauer[2], E. Berdermann[3], P. Bergonzo[4], F. Bogani[5], E. Borchi[6], A. Brambilla[4], M. Bruzzi[6], C. Colledani[7], J. Conway[8], W. Dabrowski[9], P. Delpierre[10], A. Deneuville[11], W. Dulinski[7], B. van Eijk[12], A. Fallou[10], F. Fizzotti[13], F. Foulon[4], M. Friedl[1], K.K. Gan[14], E. Gheeraert[11], E. Grigoriev[9], G. Hallewell[10], R. Hall-Wilton[15], S. Han[14], F. Hartjes[12], J. Hrubec[1,◇], D. Husson[7], H. Kagan[14], D. Kania[14], J. Kaplon[9], C. Karl[16], R. Kass[14], K.T. Knöpfle[2], M. Krammer[1], A. Logiudice[13], R. Lu[13], P.F. Manfredi[17], C. Manfredotti[13], R.D. Marshall[4], D. Meier[9], M. Mishina[18], A. Oh[16], L.S. Pan[14], V.G. Palmieri[19], M. Pernicka[1], A. Peitz[8], S. Pirollo[6], P. Polesello[13], K. Pretzl[19], V. Re[17], J.L. Riester[7], S. Roe[9], D. Roff[15], A. Rudge[9], S. Schnetzer[8], S. Sciortino[6], V. Speziali[17], H. Stelzer[3], R. Stone[8], R.J. Tapper[15], R. Tesarek[8], G.B. Thomson[8], M. Trawick[14], W. Trischuk[20], E. Vittone[13], A.M. Walsh[8], R. Wedenig[9], P. Weilhammer[9], H. Ziock[21], M. Zoeller[14]

[1] *Institut für Hochenergiephysik der Österr. Akad. d. Wissenschaften, A-1050 Vienna, Austria*
[2] *MPI für Kernphysik, D-69029 Heidelberg, Germany*
[3] *GSI, Darmstadt, Germany*
[4] *LETI (CEA-Technologies Avancees) DEIN/SPE - CEA Saclay, 91191 Gif-Sur-Yvette, France*
[5] *LENS, Florence, Italy*
[6] *University of Florence, Florence, Italy*
[7] *LEPSI, IN2P3/CNRS-ULP, Strasbourg 67037, France*
[8] *Rutgers University, Piscataway, NJ 08855, U.S.A.*
[9] *CERN, CH-1211, Geneva 23, Switzerland*
[10] *CPPM, Marseille 13288, France*
[11] *LEPES, Grenoble, France*
[12] *NIKHEF, Amsterdam, Netherlands*
[13] *Univerity of Torino, Italy*
[14] *The Ohio State University, Columbus, OH 43210, U.S.A.*
[15] *Bristol University, Bristol BS8 1TL, U.K.*
[16] *II.Inst. für Exp. Physik, Hamburg, Germany*
[17] *Universita di Pavia, Dipartimento di Elettronica, 27100 Pavia, Italy*
[18] *FNAL, Batavia, U.S.A.*
[19] *Lab. für Hochenergiephysik, 3012 Bern, Switzerland*
[20] *University of Toronto, Toronto, ON M5S 1A7, Canada*
[21] *Los Alamos National Laboratory, Los Alamos, NM 87545, U.S.A.*

◇ *representing the CERN RD42 Collaboration, e-mail Josef.Hrubec@cern.ch*

Review talk

Preprint submitted to Elsevier Preprint *25 May 1999*

Abstract

Diamond radiation sensors produced by Chemical Vapour Deposition are studied for the application as tracking detectors in high luminosity experiments. Sensors with a charge collection distance up to 250 μm have been manufactured. Their radiation hardness has been studied with pions, protons and neutrons up to fluences of 1.9×10^{15} πcm^{-2}, 5×10^{15} $p$cm^{-2} and 1.35×10^{15} $n$cm^{-2} respectively. Diamond micro-strip detectors with 50 μm pitch have been exposed in a high energy test beam in order to investigate their charge collection properties. The measured spatial resolution using a center-of-gravity position finding algorithm corresponds to the digital resolution for this strip pitch. First results from a strip tracker with a 2×4 cm^2 surface area are reported as well as the performance of a diamond tracker read out by radiation-hard electronics with 25 ns shaping time. Diamond pixel sensors have been prepared to match the geometries of the recently available read-out chip prototypes for ATLAS and CMS. Beam test results are shown from a diamond detector bump-bonded to an ATLAS prototype read-out. They demonstrate a 98 % bump-bonding efficiency and a digital resolution in both dimensions.

1 Introduction

The central part of general purpose detectors for high energy physics experiments often contains a solid state vertex detector optimized to reconstruct tracks of charged particles with high precision. In the four collider experiments at LEP at the European Laboratory for Particle Physics (CERN) these vertex detectors are composed of silicon micro-strip and silicon pixel sensors. The recently planned hadron colliders and heavy ion accelerators will deliver a very high particle flux, e.g. the luminosity of the Large Hadron Collider LHC at CERN will be of the order of 10^{34} cm^{-2}s^{-1}. Every 25 ns the detector elements positioned at the smallest radii will be traversed by about 500 charged particles from on average 18 proton-proton collisions. In addition to this load of charged particles the detectors are expected to be irradiated by albedo neutrons which are backscattered from the surrounding calorimeters. At a distance of 10 cm from the LHC beam axis the detectors are expected to receive a 1 MeV neutron equivalent fluence of 1×10^{15} cm^{-2} during 10 years of operation [1,2].

Therefore the tracking devices which are positioned closest to the interaction region must produce a fast signal (fast charge collection) and be sufficiently radiation-hard. In addition they should have a minimum of material in order to avoid multiple scattering. Carbon has a comparably low proton number which reduces multiple scattering. Few materials can withstand such a high level of radiation. Silicon strip detectors are expected to be difficult to operate

above a fluence of 1×10^{14} particles/cm^2 due to the increased leakage current and the higher bias voltage needed to compensate for the increased effective dopant density caused by radiation damage.

Since 1994 the RD42 collaboration has studied diamond produced by Chemical Vapour Deposition (CVD) for charged particle tracking [3]. Diamond detectors are potentially radiation-hard and able to survive a harsh thermal and chemically aggressive environment. The CVD diamond material studied by RD42 is produced in industry [4], grown as planar disks in research reactors and in production reactors. CVD diamond can be grown on a silicon or a metallic surface by deposition out of the gaseous phase, containing carbon, oxygen and hydrogen, under the influence of applied microwave energy. CVD diamond grows with a typical speed of 1 μm/h, depending on the operating conditions of the reactor, starting with small grains on the nucleation surface. It grows in a columnar structure with increasing lateral grain size. A thickness of 500 μm is a good target for detector applications. Thicker CVD diamonds, up to 2.6 mm, were obtained and can be lapped to a desired thickness.

Diamond has good electrical properties for use as a particle radiation detector. Its band gap is 5.5 eV. This is the reason for its high resistivity and low intrinsic charge carrier density. On average 13 eV are required to create an electron-hole pair in diamond (which is a factor 3.6 higher than in silicon). For a minimum ionizing particle, on average, 36 of these pairs are produced per micrometer of traversed diamond bulk material. Thus a diamond detector of 300 μm thickness could deliver a mean signal of 10800 electrons compared to 26700 in silicon and 39000 in gallium arsenide. The bulk leakage currents in diamond samples measured by RD42 are typically 0.05 pA/mm^2 to 1 pA/mm^2 at an electric field of 1 V/μm. The high charge carrier mobilities of 1800 cm^{2}V^{-1}s^{-1} for electrons and 1200 cm^{2}V^{-1}s^{-1} for holes mean that the charge created by a traversing charged particle will produce a fast induced signal at the contacts. The mobilities decrease above a certain field strength and cause the carrier velocity to saturate. The typical saturation field strength is 0.8 V/μm. Diamond has a dielectric constant of 5.6 which is half the value of silicon. This low dielectric constant implies a small detector capacitance at the input of the read-out amplifier. Therefore a diamond detector causes less noise than a geometrically identical silicon detector.

The diamond sensors described in this article have ohmic contacts in order to avoid polarization. These chromium or titanium contacts are covered by a gold layer to protect against oxidation and form circular dots for characterization, or strip and pixel patterns for tracking detectors. The contact preparation for diamond sensors is described in [5].

2 Characterization of Diamond Sensors

CVD diamond samples patterned with circular dot contacts on both surfaces were characterized using electrons from a ^{90}Sr source with an end-point energy of 2.28 MeV [5,6]. The specific energy loss of such electrons in diamond is close to the energy loss of minimum ionizing particles. A silicon diode behind the diamond triggers the read-out electronics. The applied electric field forces the electrons and holes of the primary ionization to drift towards the contacts. The induced charge signal from one contact is read out by a charge sensitive amplifier.

The charge collection distance of a sample is the average distance the electrons and the holes move apart under the influence of the external electric field, E, before they are trapped in the diamond material. The charge collection distance d_c is described by the formula [5,7,8]

$$d_c = \frac{\langle Q_{coll} \rangle}{\langle Q_{gen} \rangle} D = \langle Q_{coll} \rangle \, \frac{\mu\mathrm{m}}{36} \quad , \tag{1}$$

where $\langle Q_{coll} \rangle$ is the mean number of elementary charges collected at the electrodes and $\langle Q_{gen} \rangle$ the mean number of electron-hole pairs created in the total thickness D of the detector. For all samples studied so far the collected charge signal was smaller than the charge produced in the bulk since the charge collection distance is smaller than the thickness of the diamond.

The charge collection distance of the diamond samples was measured as a function of the applied electric field. As expected, it increases linearly with the electric field initially and then saturates at higher field values. The local charge collection distance in CVD diamond is not uniform along the direction of growth. The measured charge collection distance is therefore an average over the local charge collection distances across the thickness of the sample. Successive measurements of the charge collection distance on samples which were thinned in several steps from the nucleation side show a linear increase with the removed material thickness [9]. This implies that the local charge collection distance is close to zero at the nucleation side and rises linearly to a maximum at the growth side.

When a diamond sample is exposed to ionizing radiation its charge collection distance increases with the absorbed dose ("pumping"). At about 1 kRad the charge collection distance saturates at a value typically 1.3 to 2 times higher than before irradiation. The pumping of the diamond is explained by active traps in the diamond bulk which are filled by the charge carriers created by the ionization. When kept in dark the diamond remains in the pumped state. Exposure to certain frequencies of light de-pumps the diamond to its initial

state. The pumping can then be repeated.

Over the past few years about 150 diamond samples have been characterized. In an iterative process between the RD42 collaboration and the manufacturers, the procedures to produce CVD diamond material with good charge collection properties have been refined. Figure 1 shows the charge signal distribution for a 432 μm thick diamond (UTS-5) in the pumped state at an electric field of 1 V/μm as measured with a ^{90}Sr source. The observed Landau distribution is well separated from zero and peaks at a most probable value of 6000 electrons. The mean signal of the distribution amounts to 8330 electrons which corresponds to a charge collection distance of 235 μm. The ratio between the mean signal and the most probable signal is close to 1.4, this value is characteristic for the shape of the charge distribution for many of the diamond samples studied.

Figure 2 shows the increase in charge collection distance of CVD diamond over recent years. In 1991 the charge collection distance was at a value of less than 5 μm and now diamonds with a charge collection distance of up to 250 μm are available.

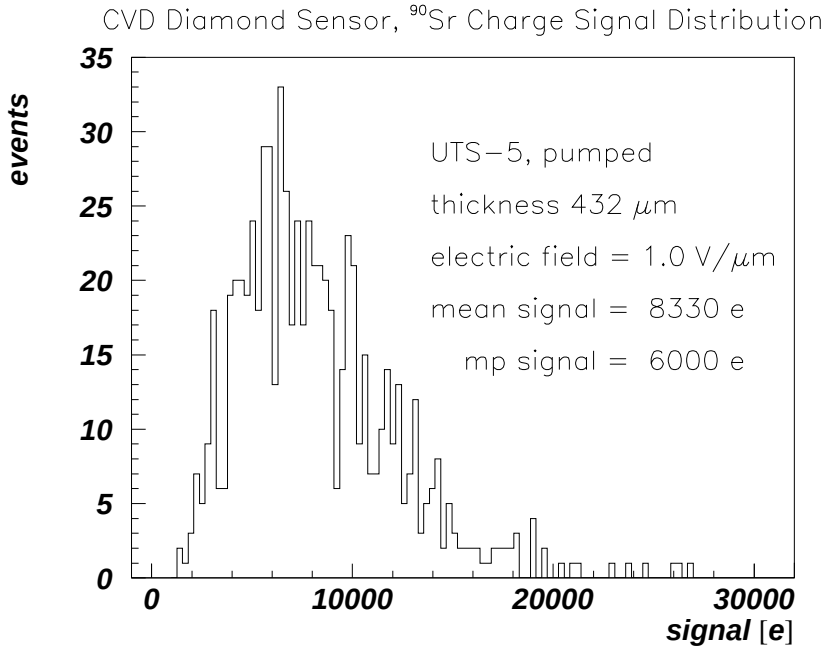

Fig. 1. Charge signal distribution from the diamond sample UTS-5 measured using a ^{90}Sr source.

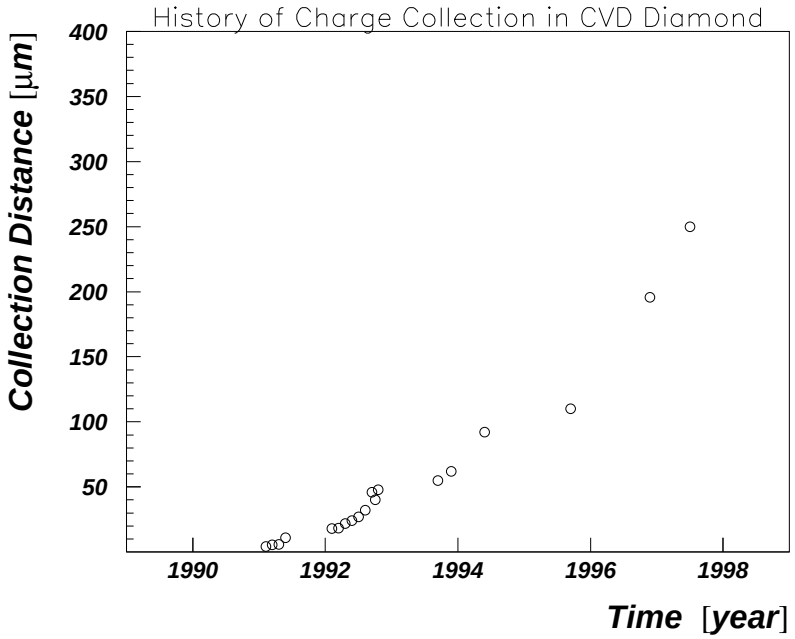

Fig. 2. History of the charge collection distance achieved from year 1991 to 1997.

3 Irradiation Studies

The radiation resistance of diamond to electro-magnetically interacting radiation like photons and electrons up to 10 MRad and 100 MRad, respectively, has been demonstrated in the past [10]. No decrease of the charge collection distance in the pumped state was observed.

Several CVD diamond samples have been irradiated with pions, protons and neutrons [11]. In all three cases the samples were kept at room temperature and operated with a bias voltage between 100 V and 300 V. During irradiation the particle induced current was measured for the individual samples. At different particle fluences the irradiation was stopped and the charge collection distances of the samples were measured.

3.1 Irradiation with Pions

Over the past four years CVD diamond samples have been irradiated with 300 MeV/c pions at the Paul Scherrer Institute in Switzerland. At 300 MeV/c the nuclear cross-section of the π^+ with the protons inside the carbon nuclei reaches a maximum (Δ resonance). The accelerator delivered a quasi continu-

ous particle beam with a flux of up to 2.5×10^9 $\pi\mathrm{cm}^{-2}\mathrm{s}^{-1}$. The highest fluence accumulated on one diamond sample was 1.9×10^{15} $\pi\mathrm{cm}^{-2}$. Before irradiation the diamond samples had charge collection distances of up to about 170 μm in their electron pumped state. The absolute pion fluence absorbed by each sample was measured by an activation method using aluminum foils.

Figure 3 shows for one diamond sample the charge signal distributions in the pumped state before irradiation and after the absorbed pion fluence of 1.1×10^{15} $\pi\mathrm{cm}^{-2}$. At this fluence the mean charge signal is decreased by 30 % due to the loss of high signals, as indicated by fewer entries in the high tail of the Landau distribution. The region of small signals is less affected and therefore the most probable value of the charge signal distribution is decreased by less than 15 %.

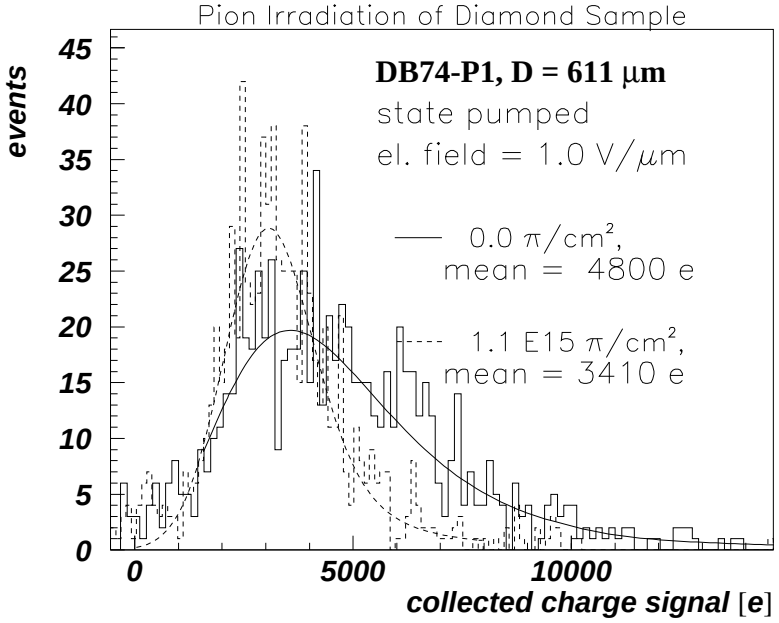

Fig. 3. Charge signal distribution in a diamond sample before irradiation and after the pion irradiation.

Figure 4 shows the charge collection distance of the samples at different accumulated pion fluences normalized to their collection distance measured before irradiation. It is important to notice that the charge collection distance is derived from the mean value of the charge signal distribution. The dark current of the samples, typically of the order of 1 pA/mm^2 before irradiation, was slightly reduced after the exposure.

When a non-irradiated diamond sample is exposed to a ^{90}Sr source a certain dose is required to reach the pumped state where the charge collection distance reaches a maximum (see section 2). This dose increased linearly with the

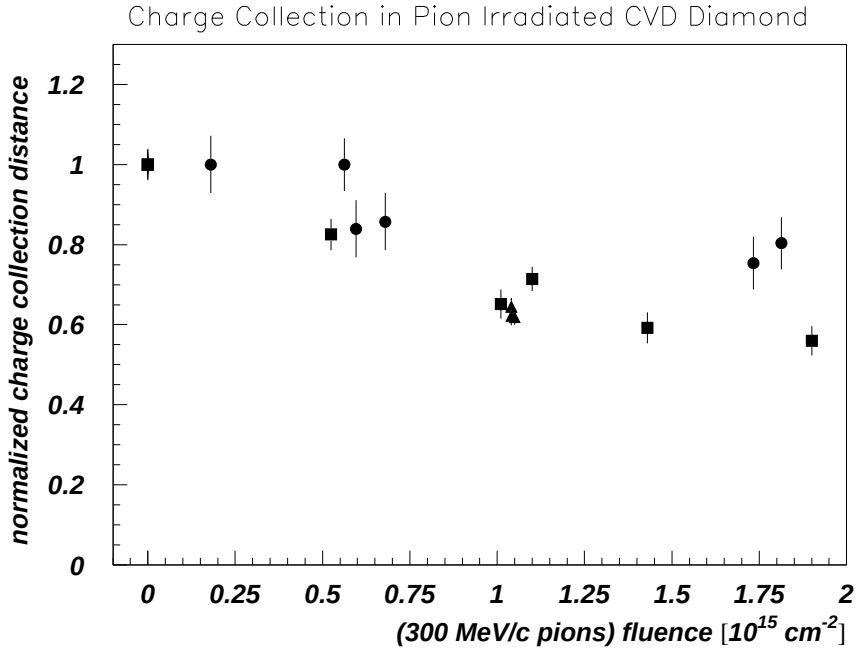

Fig. 4. Charge collection distance on diamond samples as a function of the pion fluence. For each sample the charge collection distances are normalized to the electron pumped value before pion irradiation.

received fluence in the pion irradiation. This observation can be attributed to new traps introduced in the diamond bulk which have to be filled with additional charge carriers.

3.2 Irradiation with Protons

The irradiation of CVD diamond samples with 24.2 GeV/c protons was performed at the Proton Synchrotron at CERN up to a fluence of 5×10^{15} $p\mathrm{cm}^{-2}$ [12]. The average flux was 2.9×10^{10} $p\mathrm{cm}^{-2}$ per spill with 2 or 3 spills, each of 300 ms length, in a 14 s time interval. For the fluence determination the same activation method as for the pion irradiation was used.

Figure 5 shows the relative charge collection distance as a function of the received proton fluence for diamond samples with a charge collection distance of about 100 μm before irradiation. After irradiation with 0.9×10^{15} $p\mathrm{cm}^{-2}$ the charge collection distance is increased by a small amount when compared to the pumped value before irradiation. At the next measurement at 3×10^{15} $p\mathrm{cm}^{-2}$ a reduction of 10 % compared to before the proton irradiation is observed. From there on the charge collection distance decreases linearly and

reaches 60 % of its unirradiated value at a fluence of 5×10^{15} $p\mathrm{cm}^{-2}$. The linear fit to the charge collection distance values above 3×10^{15} $p\mathrm{cm}^{-2}$ intersects the ordinate value one at a fluence of $\approx 2 \times 10^{15}$ $p\mathrm{cm}^{-2}$. The most probable value of the charge signal distribution at a fluence of 5×10^{15} $p\mathrm{cm}^{-2}$ is decreased by only 20 % when compared to before irradiation.

Since each proton spill lasted only 300 ms the ON-spill current was measured during this time-span and the OFF-spill current was recorded in the breaks between spills. The difference between these two quantities is the proton induced current which correlates well with the proton flux. The OFF-spill current is negligibly small and remained constant during irradiation for all samples. This is clearly in contrast to a silicon diode irradiated in parallel, for which the OFF-spill current grew constantly with the received proton fluence.

For the diamond samples the observed proton induced current is consistent with the predicted value from the charge collection distance. This agreement was verified with diamond sensors equipped with a guard ring around the dot contact to define precisely the active area. The guard ring was kept at ground potential during the irradiation.

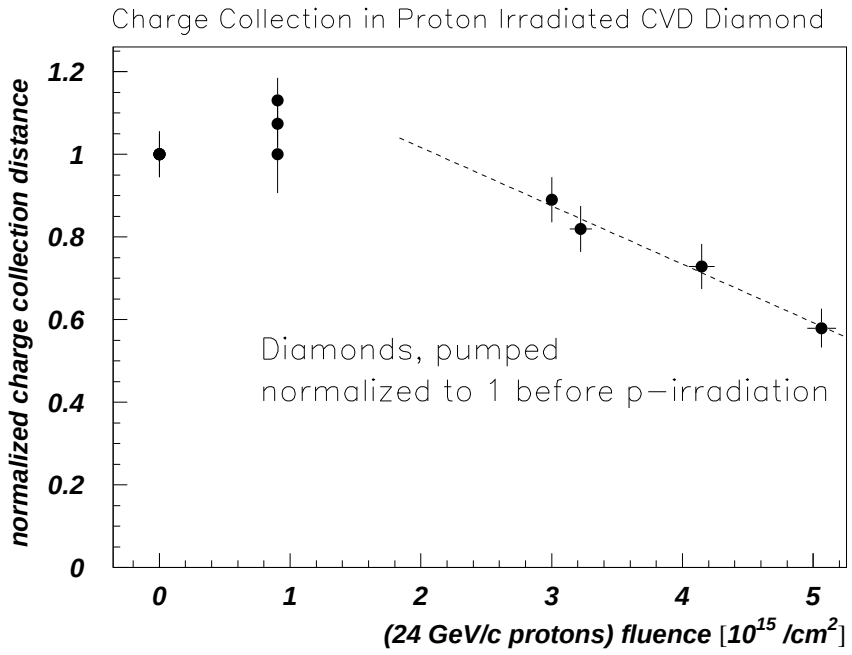

Fig. 5. Charge collection distance on diamond samples as a function of the proton fluence. For each sample the charge collection distances are normalized to the electron pumped value before proton irradiation. The dashed line corresponds to a fit for the values above 3×10^{15} $p\mathrm{cm}^{-2}$.

The irradiation of diamond samples with neutrons was performed at the ISIS facility at the Rutherford Appleton Laboratory in England [13]. Thermal neutrons with kinetic energies below 10 keV and neutrons with energies peaking at 1 MeV were delivered, the mean flux of neutrons above 10 keV was about 1.7×10^8 $n\mathrm{cm}^{-2}\mathrm{s}^{-1}$ at the position of the samples. The samples had charge collection distances of up to 70 μm before irradiation.

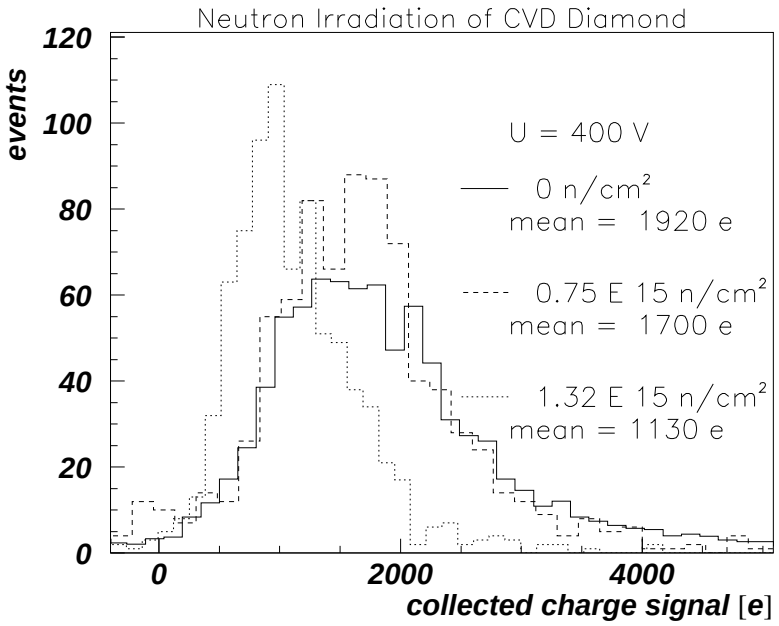

Fig. 6. Charge signal distribution in a diamond sample before irradiation and after two neutron irradiations.

Figure 6 shows the charge signal distributions measured on a diamond sample before irradiation, after 0.75×10^{15} $n\mathrm{cm}^{-2}$ and after 1.35×10^{15} $n\mathrm{cm}^{-2}$. At a fluence of 0.75×10^{15} $n\mathrm{cm}^{-2}$ the mean value of the distribution is decreased by ≈ 15 %, but the most probable value is unchanged. The mean value of the distribution after 1.35×10^{15} $n\mathrm{cm}^{-2}$ is reduced by 40 % and the most probable value is also significantly decreased [11].

The induced currents of two diamond samples and of a silicon diode, kept at 18 °C and −8 °C respectively, are plotted as a function of time during irradiation in Figure 7. One diamond sample was positioned close to the spallation source and received 1 MeV neutrons and thermal neutrons. The induced cur-

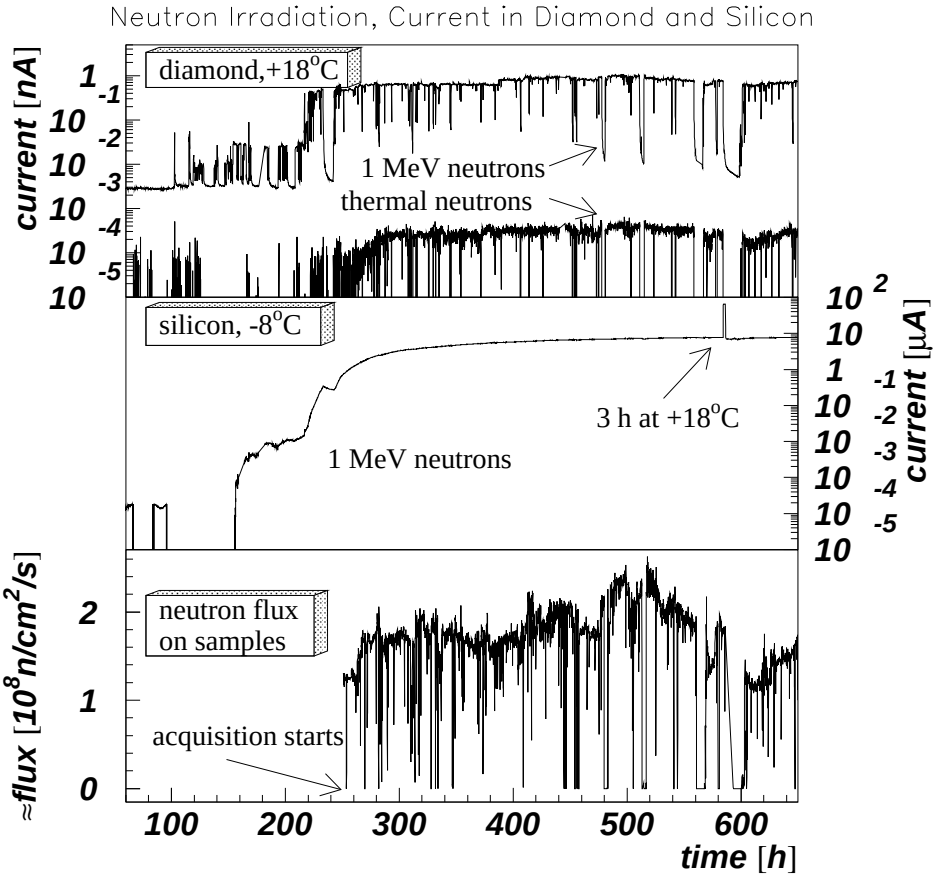

Fig. 7. Neutron induced current during irradiation in two diamond samples and in a silicon diode, together with the neutron flux.

rent was several hundred pA when neutrons were present. It correlates with the neutron flux at this location, which is also shown in Figure 7, and returns to a 100 times smaller value during beam-off periods. The other diamond was irradiated far from the source and therefore received thermal neutrons only. The sample exposed to the 1 MeV neutrons shows an induced current which is higher by three orders of magnitude than that in the sample irradiated with thermal neutrons only. This is caused by inelastic interactions of the neutrons with carbon or hydrogen in the diamond.

The induced current in the silicon diode, which is displayed in the center of Figure 7, increases non-linearly from a few pA to 10 μA after 600 hours of irradiation. During the beam-off periods the current of the silicon diode decreases only slowly due to annealing. The spike in the current after 580 hours was caused by an accidental warming.

4 Diamond Sensors as Micro-strip Detectors

CVD diamond strip detectors with good charge collection distance have been used to study the charge collection mechanism and to measure their spatial resolution in a pion test beam at CERN. On one side these detectors have a pattern of strips with 50 μm pitch and a guard ring around this structure. The other surface of the diamond is covered by a uniform metal contact. The metal to produce the ohmic contact to the diamond is chromium covered by a gold layer.

The diamond detectors were placed inside a beam telescope with eight planes of silicon strip detectors. Each read-out strip of the telescope is bonded to the input of a VA2 read-out chip [14,15] and connected to a Sirocco-ADC. Four planes of silicon detectors with x- and y-coordinates form a station and the resulting two stations are positioned 18 cm apart. Each plane of the telescope consists of a silicon strip detector with 256 read-out strips of 50 μm pitch and floating strips in between. The standard deviation of the residual distribution for each plane of the telescope is about 2 μm. The uncertainty on the predicted position at the center of the telescope is better than 2 μm.

In the analysis the diamond detector is first aligned to the coordinate system of the telescope. For each read-out strip the charge signal is determined by the difference between the raw pulse height and the pedestal value (both for the same strip), after correction for common mode variations. The total charge of a hit can then be calculated by summing the charge of several strips closest to the track prediction, independent of any threshold (*transparent analysis*). In a *cluster analysis* a hit is found by searching for the seed strip with the highest charge signal and exceeding a given signal-to-noise threshold. To form a hit cluster, neighboring strips are included if their charge signal is above a signal-to-noise threshold which is typically one third of the threshold for the seed strip. The cluster charge is the sum of all strip charges in the cluster. The position of the hit cluster in the diamond detector is calculated by a center-of-gravity method.

4.1 Read-out with Viking Type Electronics

The 432 μm thick diamond UTS-5, described in section 2, was re-metallized as a strip detector with 50 μm pitch and studied in a 100 GeV/c pion beam. For this experiment the detector was bonded to a VA2 read-out chip. For 128 channels this chip performs charge integration and signal shaping with a characteristic peaking time of 2 μs. The series noise at 2 μs signal shaping time is ENC $\approx 82\ e^- + 14\ e^-$/pF.

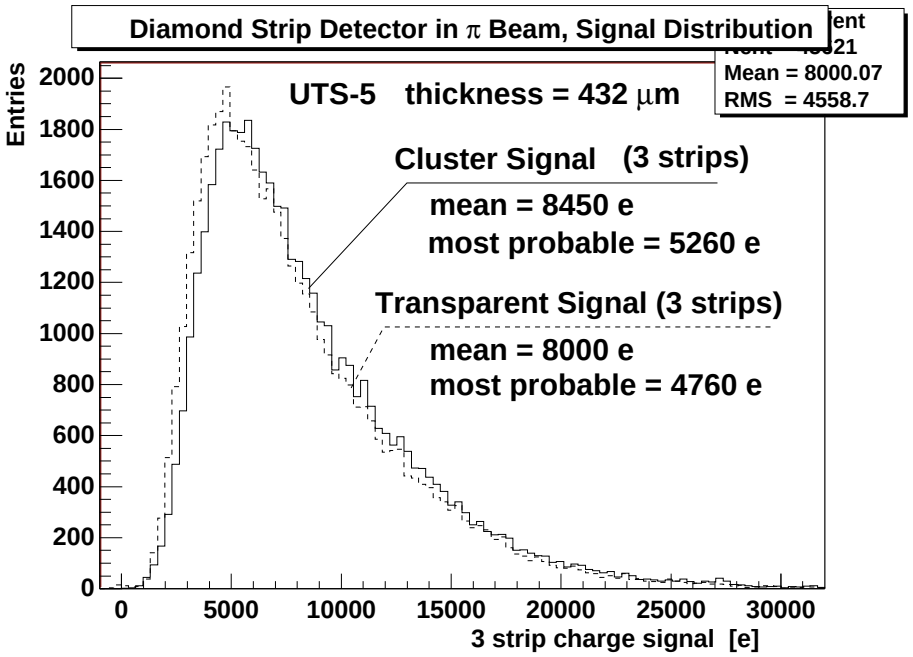

Fig. 8. Distribution of charge signals measured from the diamond strip detector UTS-5.

The detector was biased with 432 V which corresponds to an electric field strength of 1 V/μm. Figure 8 shows the charge signal distributions from the cluster analysis and the transparent analysis, both including three strips. The two distributions have the same shape, the charge signal is well separated from zero and starts at about one third of the most probable value. The calibration constant for the read-out chain, including the gains of the Sirocco-ADC and the VA2 amplifier, was determined by a measurement of the known signal of a silicon strip detector in the beam. The mean signal for the UTS-5 diamond tracker is 8450 electrons as determined in the cluster analysis and 8000 electrons in the transparent analysis. These measurements are in good agreement with the charge signal distribution obtained with a source as described in section 2. Based on the cluster analysis, the most probable value for the signal-to-noise ratio is 46-to-1.

Using a center-of-gravity method to determine the hit position in the diamond strip detector the track residual is Gaussian distributed and the fit gives a spatial position resolution of (15.2 ± 0.1) μm. Correcting for the error in the track projection from the reference planes the position resolution of the diamond is found to be 14.9 μm. This corresponds to the expected digital resolution for a 50 μm pitch strip detector using this algorithm.

Figure 9 shows the pulse height measured for the strip closest to the track prediction as a function of the distance between the center of this strip and the track prediction (U_{track}). The metallization for the central strip extends

from -12.5 μm to +12.5 μm, the regions below -37.5 μm and above +37.5 μm are covered by the adjacent strips. In this figure the crosses indicate the mean value of the pulse-height distribution determined for each bin of U_{track}. This illustrates that the pulse height is almost independent of the track position for tracks passing through the metallization of a strip. For tracks passing in between strips a linear behavior is suggested for the pulse height. A similar analysis of the charge measured for hit clusters showed that no charge loss is observed for tracks which are predicted to pass in the region between strip metallizations. Therefore it is envisaged to study strip detectors with narrower strip metallization in order to take advantage of charge sharing and to optimize the position resolution of diamond strip detectors.

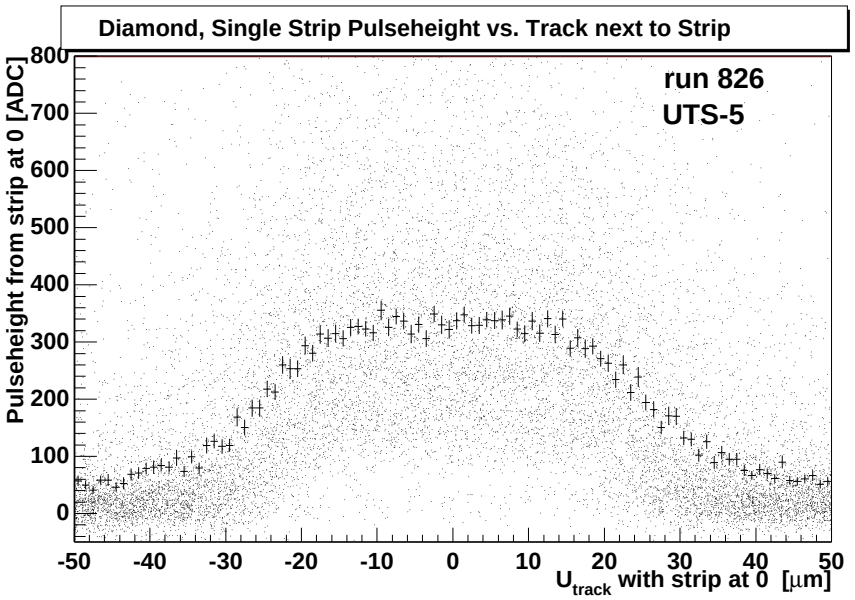

Fig. 9. The charge signal distribution (dots) and its mean (crosses) measured on the strip nearest to the track as a function of the distance between the strip and the track.

4.2 Read-out with fast, LHC Compatible Electronics

In another beam test, diamond strip detectors were read out with the 32-channel DMILL/SCT32A read-out chip [16]. This fast electronics is compatible with the 25 ns spill structure of the LHC accelerator and the timing specifications for triggering. Each channel of the SCT32A, which was developed as a prototype for the ATLAS experiment in a radiation-hard technology, consists of a bipolar preamplifier and a signal shaper followed by a 112 cell analog pipeline and a 32-channel multiplexer. The shaper has a signal peaking time between 21 and 25 ns, depending on the capacitive load. The single channel equivalent noise charge of the chip is ENC $\approx 650\ e^- + 70\ e^-/\mathrm{pF}$.

The analog pipeline samples the output signal of the shaper at the 40 MHz clock frequency. In the beam test the delay time between the trigger signal from a scintillator and the clock phase for the pipeline was measured with a TDC. In a transparent analysis, summing the signal of the three strips closest to the track prediction, the maximum signal output was found in a 6 ns wide time window. The charge signal distribution in this selected time interval is shown in Figure 10 for the diamond strip detector D39. The mean signal of the distribution is 59 ADC-counts. The noise on a strip was determined to be 6.2 ADC-counts corresponding to about 750 electrons. Therefore the mean signal-to-noise ratio is 10-to-1 and the most probable value for this quantity is 5-to-1. The spatial resolution for this detector using a center-of-gravity method was found to be (21 ± 2) μm.

It should be noted that the SCT32A chip was optimized for silicon strip detectors. A new design, the SCT128LC, is optimized for the relatively lower detector capacitance of diamond strip detectors. This chip has 128 channels and a pipeline with 128 cells and new functions for control and monitoring. Simulations predict a noise performance of ENC = 600 to 700 electrons for a 6 cm long diamond strip detector.

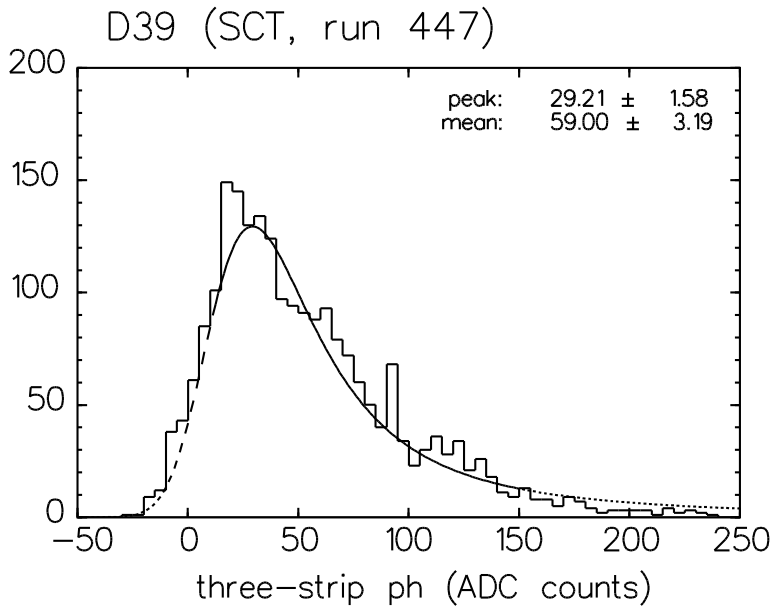

Fig. 10. Distribution of charge signals measured on a diamond strip detector with DMILL/SCT32A read-out. The smooth curve is a restricted fit to the distribution.

In order to investigate the behavior of diamond detectors with a surface area approaching the size of detectors to be used in a physics experiment, the first diamond strip detectors with 2×4 cm^2 area have been produced. One detector had a thickness of 650 μm and was metallized with a pattern of 3.8 cm long strips at a pitch of 50 μm. For the test in the 100 GeV/c pion beam the strips were read out by a VA2 chip.

The measured charge signal distribution for this detector from a transparent analysis, summing the five strips closest to the track prediction, is shown in Figure 11. The signal distribution is well separated from zero, with a mean value of the signal distribution at 5200 electrons at 0.3 V/μm electric field. This agrees with the measurement using a ^{90}Sr source. The charge collection distance of this sample is therefore 145 μm at 0.3 V/μm. The small pedestal contribution is due to a strip with an interrupted metallization which was not excluded by the fiducial region cuts. The signal-to-noise ratio for the most probable charge signal of this detector is 23-to-1. In the fiducial region selected for the analysis the spatial resolution was measured to be 14 μm with the center-of-gravity method. This is equivalent to the digital resolution expected for a detector with 50 μm strip pitch using this algorithm.

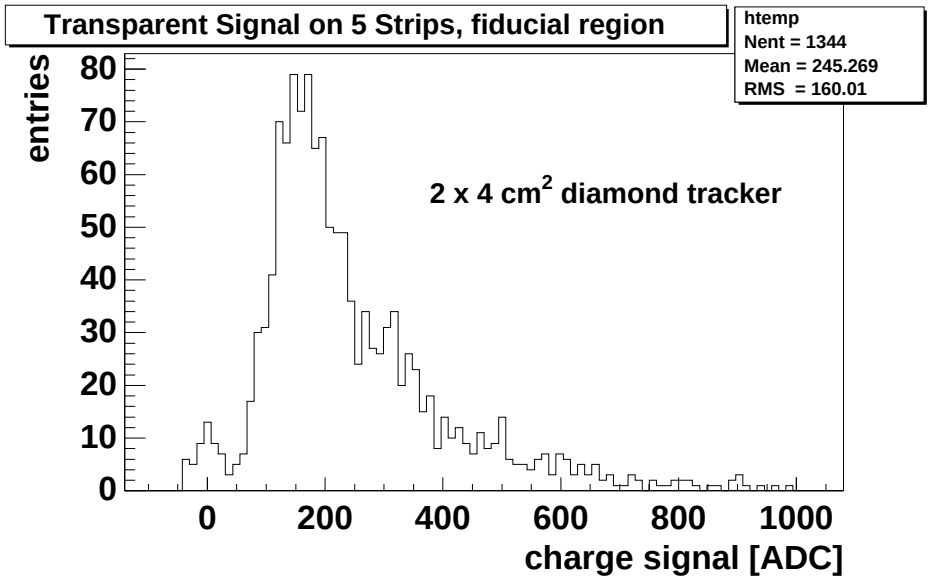

Fig. 11. Charge signal distribution from the first 2×4 cm^2 diamond strip detector measured in a transparent analysis summing five strips.

5 Diamond Pixel Detectors

The first 16×16 matrix of 150×150 μm^2 diamond pixels was tested in 1996 [6]. The pixels were wire-bonded to a fan-out on a glass substrate, enabling the read-out with a VA3 read-out chip. This chip has similar characteristics to the VA2 chip used in the tests described in the previous section. The measured mean signal-to-noise ratio was 27-to-1 and the position resolution in both dimensions was consistent with the digital resolution of the pixels.

Both high luminosity LHC experiments, ATLAS and CMS, plan to install pixel detectors as the innermost charged particle tracking devices around the interaction region for pattern recognition and vertexing. Each pixel element has to be read out by an amplifier and a shaper. A sparsification logic has to select the pixel elements containing a hit exceeding a well adjusted threshold to reduce the number of data words to be stored subsequently. Because the individual pixel element in a matrix has to be connected via a bump-bond to a read-out cell on the read-out chip, the geometrical dimensions of the elements on the sensor and on the chip have to be properly matched. The design of pixel read-out electronics is still evolving, therefore first attempts were undertaken to equip pixel detectors based on CVD diamond with the existing prototype chips developed for the two experiments.

5.1 Sensor Preparation

The bump-bonding procedure for bumps at the 10 μm scale is not simple to develop. The different diamond pixel sensors prepared during the last year and matching the requirements of the prototype read-out chips of ATLAS and CMS are listed in Table 1. The dimensions of the pixel arrays, the contact metallization together with the bump-bonding material are listed for each sample. Sections of the contact structure on the different diamond pixel sensors are shown in Figure 12. The contact positions for the bump-bond on each pixel are offset from the pixel centers in a regular way. This offset is defined by the structure of the read-out chips, grouping the pixels in a double column architecture.

The pixel cells of the metallization pattern for CMS, as shown in Figure 12a, are made with Cr-Au contacts with a size of 100×100 μm^2. Including the gaps between the metallized squares this results in a pitch of 125 μm for both dimensions of the diamond surface. The gold surface of the pixel cells is covered by a 0.2 μm thick passivation layer necessary for the following bump-bonding steps. This passivation layer has a circular hole of ≈ 20 μm diameter offset from the pixel center. The diamond surface in the gaps between the pixel

Table 1
Overview of diamond pixel sensors produced to match pixel read-out chips of CMS and ATLAS.

	pixel cell size [μm^2]	diamond substrate size [μm^2]	metallization [elements]	passivation [yes/no]	bump-bonding metal
CMS	125 ×125	3725 × 4725	Cr-Au	yes	In
ATLAS/1	50 ×433.4	3800 × 5800	Cr-Ni-Au	yes	Sn-Pb
	50 ×433.4	3800 × 5800	Ti-W/Ti-Ni-Au	no	Sn-Pb
ATLAS/2	50 ×433.4	3800 × 5800	Ti-W	no	In
ATLAS/3	50 ×536	4000 × 8000	Ti-W	no	In

metallization is not covered by the passivation layer in order not to bypass the high resistivity of the diamond by an insulator with lower resistivity.

First bump-bonding tests were performed at the Paul Scherrer Institute in Switzerland. Indium metal was deposited from the vapour phase using a metal mask with 80 μm holes centered with the holes in the passivation layer. This sample was then pressed with about 1 μg/μm^2 against a silicon substrate which was heated to 170 °C. As a result (see Figure 12a) the indium contracts during cooling and is attached as a pearl to the gold contact of the pixel cell through the hole in the passivation layer. Further improvements of this procedure are being tested to finally produce a real bump-bonded diamond pixel detector prototype.

The metallization patterns of the diamond pixel sensors to be read out with the ATLAS/1 and ATLAS/2 electronics are geometrically identical (see Figure 12b). The basic difference is the surface preparation for the bump-bonding used in industrial processes. In the case of ATLAS/1 the gold is melted and the Sn-Pb solder connects to the nickel layer. A radiation-hard DMILL version of the corresponding pixel read-out chip is available. For ATLAS/2 the contacts are produced as Ti/W metal layers for indium bump-bonding which is industrially used for the processing of entire wafers. It is anticipated that the ATLAS/2 chip will have a threshold as low as 1800 electrons.

The slightly longer pixel cells of ATLAS/3 are arranged in a bricked geometry as shown in Figure 12c, where part of the guard ring is also visible. This arrangement can improve the position resolution in the direction of the shift by a factor of two when charge is shared between the pixels of adjacent rows. Titanium as a first metallization layer makes a very good contact to the diamond surface and tungsten is an inert metal which is commonly used in integrated

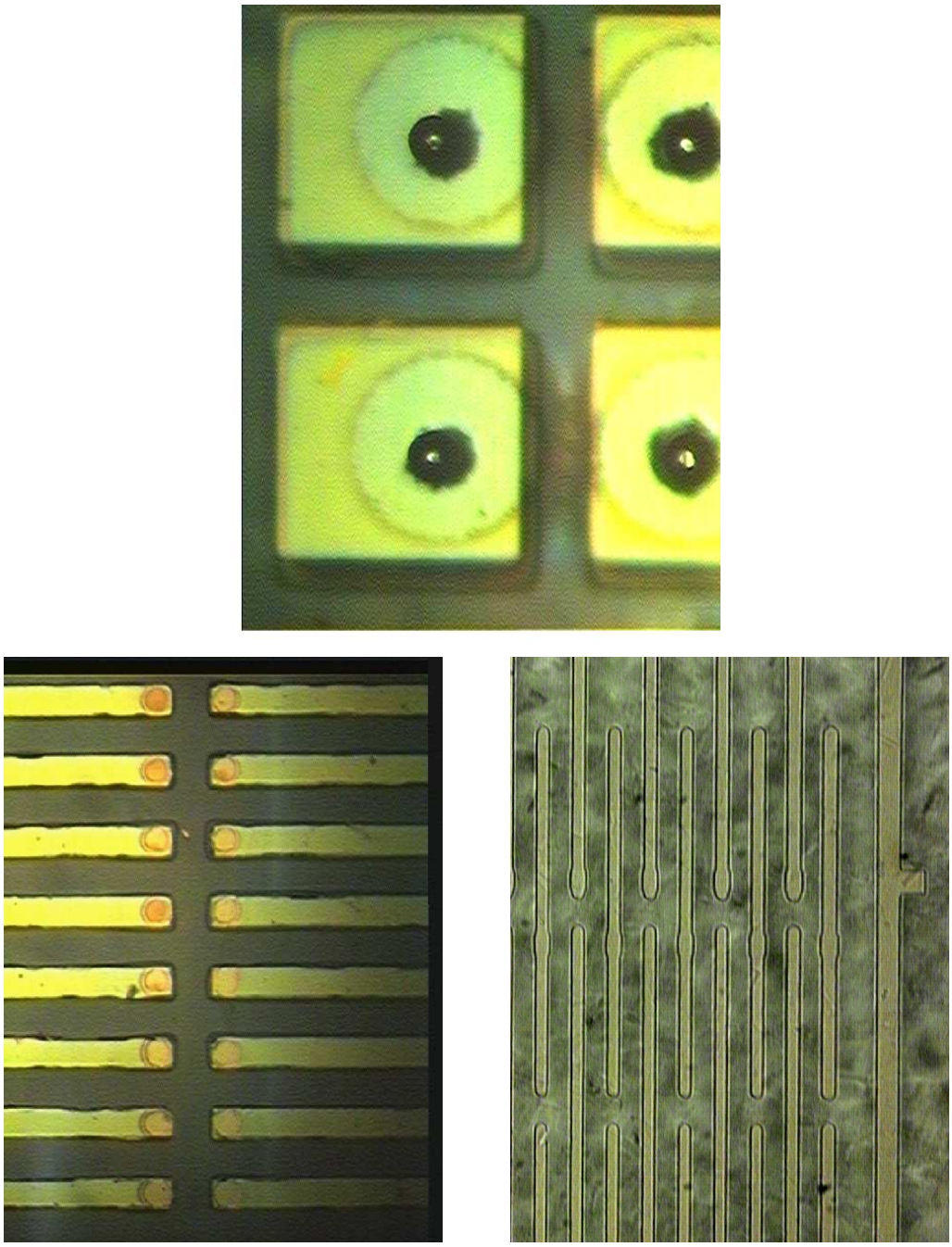

Fig. 12. Photographs: a) Four pixel cells of a CMS diamond pixel sensor. b) Diamond sensor for ATLAS/1. c) Diamond sensor for ATLAS/3.

circuit processing.

The ATLAS/3 diamond pixel sensor was successfully bonded to a read-out chip at BOEING [17]. This work was done in collaboration with the ATLAS group at the Lawrence Berkeley National Laboratory. A visual inspection and consecutive tests with a ^{107}Ru beta source led to the conclusion that all pixels

were connected and functioning. In order not to damage the read-out chip which is only available in a non-radiation-hard version the diamond sensor was not brought to its pumped state. The same statement applies also to the measurements done in the test beam and described in the following section.

5.2 Beam Test Results

The ATLAS/3 pixel detector was studied in the test beam area equipped with the silicon reference telescope (see section 4). The diamond sensor had a thickness of 610 μm and was biased with a bias voltage of 450 V. Tracks from 200000 perpendicularly incident particles were collected and analyzed to produce a pixel population map (Figure 13) and to study the measured charge signal distribution and the spatial correlations between the pixel tracker and the reference telescope.

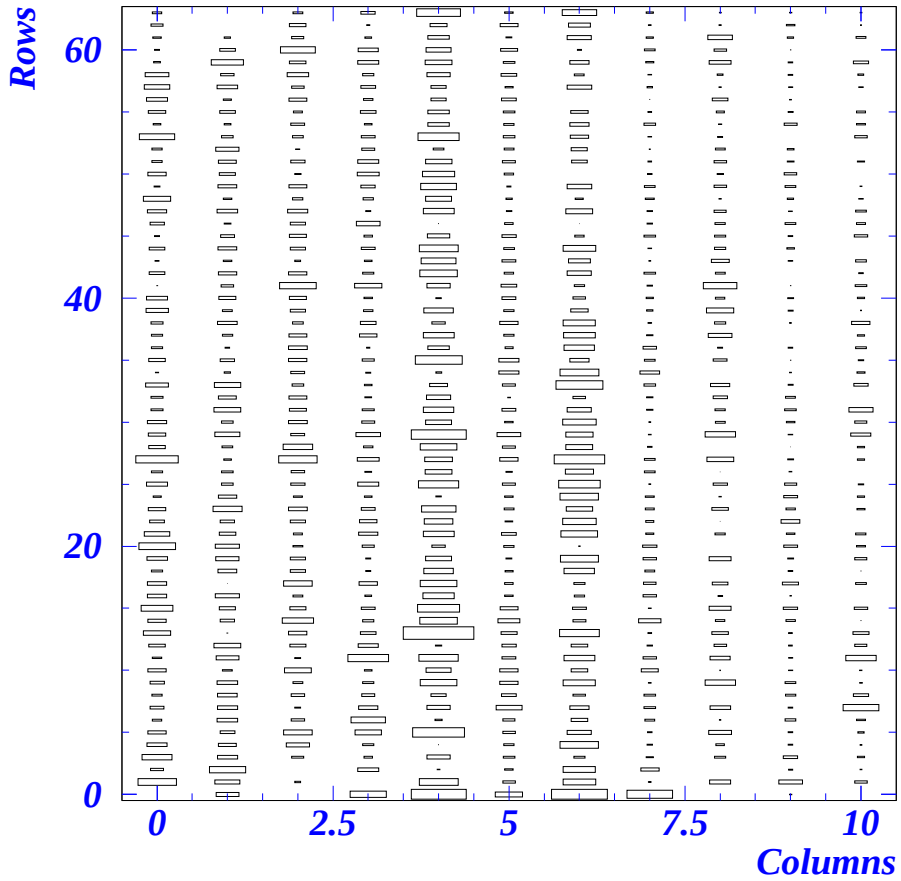

Fig. 13. Number of hits per pixel seen in a test beam in April 1998.

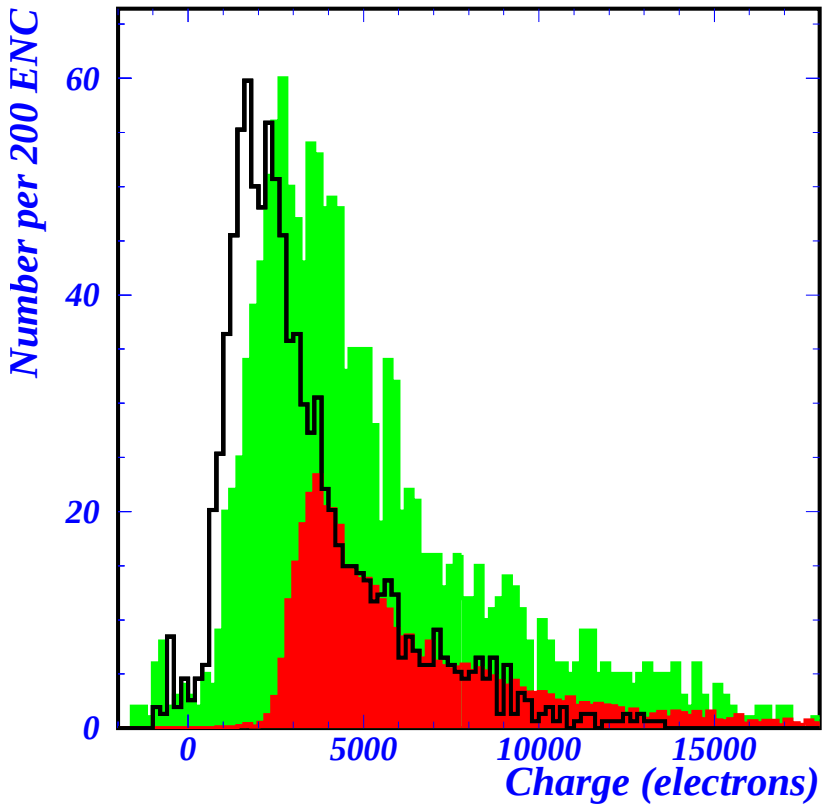

Fig. 14. Comparison of the charge observed for the pixel tracker in the unpumped state (black histogram) with that seen in the pumped state for the same diamond when it was instrumented as a strip tracker in 1997 (light gray histogram). Based on this observed charge (light gray histogram), the open histogram is a prediction for the charge expected in the unpumped pixel tracker.

The size of the boxes in Figure 13 is proportional to the number of hits found for each pixel. Clearly there are only very few pixels without a recorded hit. The right part of the plot exhibits a lower hit population which might be due to a slightly displaced beam position or to a variation of the threshold of the read-out chip. Because they contain many hits resulting from threshold problems the columns 4 and 6 have been excluded from the following analysis. The content of Figure 13 can be translated into a distribution of the number of pixels containing a given number of hits. The number of pixels without any hit recorded and statistical arguments involving the number of pixels containing only a few hits lead to the conclusion that 98 % of the pixels are successfully bonded and operational. The same analysis for the left part gives the same result.

In Figure 14 the black histogram shows the charge signal distribution measured

for the ATLAS/3 detector in its unpumped state. The distribution is distorted on the left rising edge and its area corresponds to only 25 % of the number of entries expected from the track extrapolations in the reference telescope. This result can be interpreted as the effect of the applied threshold. The diamond sample used for the ATLAS/3 pixel tracker was previously tested as a strip detector metallized with 50 μm strip pitch. The corresponding charge signal distribution measured with this strip tracker in its fully pumped state is displayed as the light gray histogram in Figure 14. This distribution can be scaled down by 40 % (open histogram in Figure 14) corresponding to the prediction for this sample in the unpumped state. The comparison of this prediction with the charge distribution measured for the pixel tracker (black histogram) leads to the conclusion that the pixel tracker was operated with a maximum pixel threshold of 4000 electrons.

The hit positions, measured with the diamond pixel tracker as the center of the pixel with the highest signal, are properly correlated with the track predictions from the silicon reference telescope. Figures 15a and 15b show the difference between the position measured with the pixel detector and the theoretical prediction. Since charge sharing between pixels was not taken into account the resolution in the direction of the large pixel dimension (Figure 15a) corresponds to the digital resolution of the 536 μm long pixels. In the direction of the small pixel dimension the position resolution obtained is 14.8 μm (Figure 15b), consistent with the digital resolution for the 50 μm pixel width. In both distributions the minimal tails beyond the main peak show that very few hits found in the pixel detector are not correlated with a charged particle track.

6 Summary

Over the past few years the RD42 collaboration has made excellent progress in improving the quality of CVD diamond tracking detectors in close collaboration with industry. For minimum ionizing particles, recently delivered samples give mean charge signals of 9000 electrons, corresponding to a charge collection distance of 250 μm. High quality CVD diamond is produced by lapping the substrate side of the sensor, removing material with low charge collection distance. The diamond growing process has been successfully transferred to a production reactor aiming for series production of sensors with a surface area appropriate for application in physics experiments.

The irradiation studies with pions, protons and neutrons indicate that the tested CVD diamond material is sufficiently radiation-hard for applications in tracking detectors at small radii in high luminosity experiments. At the high fluences reached for the three particle types, the onset of radiation damage

is observed as a loss of signals in the high tail of the Landau distribution. The region of small signals is less affected and therefore the most probable

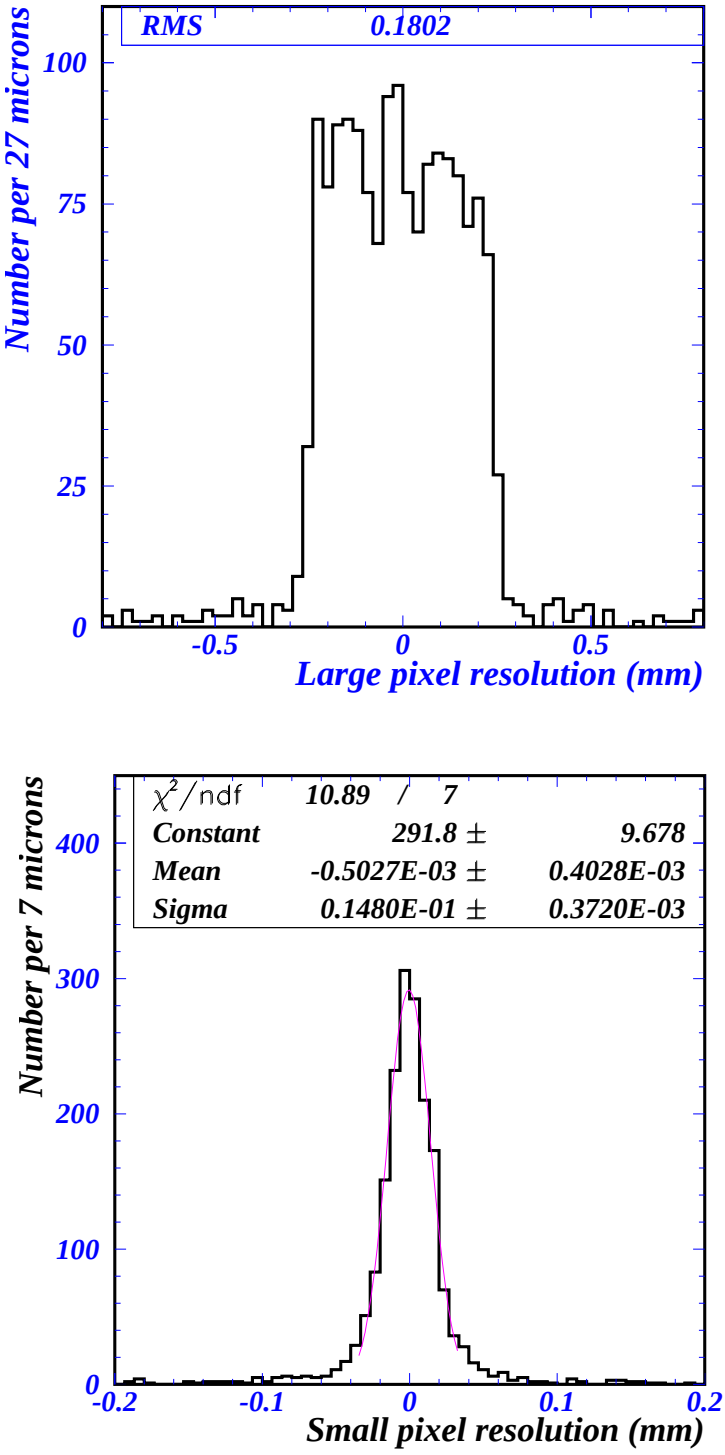

Fig. 15. The position resolution of the pixel detector prototype a) in the x (long pixel) view and b) in the y (short pixel) view.

value of the charge signal distribution is reduced to a lesser extent than the mean value. This effect may be partially explained by the fact that the local charge collection distance in CVD diamond is highest close to the growth side. Additional traps, which are randomly introduced in the diamond bulk, cause a bigger fractional reduction of the high signals from the regions with good charge collection properties compared to the small signals from regions with poor charge collection.

Diamond micro-strip detectors with a pitch of 50 μm and read out with "slow" electronics (2 μs) have been exposed to a test beam and give charge signal distributions which are well separated from zero. Small trackers with 1 cm^2 area and operated at 1 V/μm yield a most probable signal-to-noise ratio of 46-to-1. For trackers read out with LHC compatible electronics the signal-to-noise ratio in a test beam is already approaching 10-to-1, but the chip has still to be optimized for the low capacitance of the diamond detectors. Test beam results from the first detector with 2×4 cm^2 surface area, read out with "slow" electronics and operated at 0.3 V/μm, give a most probable signal-to-noise ratio of 23-to-1. Further detectors of this type have been produced recently and tested with very good results. A study of the homogeneity of the charge collection properties across the surface is envisaged and needs to be performed with high statistics on the scale of a few tens of micrometers in the lateral dimensions.

The development of diamond pixel sensors for the different prototype read-out electronics chips of ATLAS and CMS has made good progress in the difficult area of sensor metallization for connection with the bump-bonding technique. The first results from a pixel detector (ATLAS/3) in a test beam demonstrate 98 % efficiency for the bump-bonding of the pixels and digital spatial resolution for the track measurement in both dimensions. The measured charge signal distribution for this detector shows that diamond sensors with even higher charge collection distance need to be combined with low noise read-out chips in order to achieve tracking with good efficiency and a sufficiently high signal-to-noise ratio in an experiment.

The research of the RD42 collaboration is aiming for a series production of CVD diamond tracking detectors with optimal properties for use in high luminosity experiments at the LHC and at the Tevatron at Fermilab. First proposals have already been submitted for the beam monitoring of heavy ion beams at GSI-Darmstadt and for a research program for a vertex detector upgrade of CDF at Fermilab [18].

References

[1] ATLAS Collaboration, Inner Detector Technical Design Report, CERN/LHCC 97-16, ATLAS TDR 4, 30 April 1997.

[2] CMS Collaboration, Tracker Technical Design Report, CERN/LHCC 98-6, CMS TDR 5, 15 April 1998.

[3] The RD42 Collaboration, "R&D Proposal, Development of Diamond Tracking Detectors for High Luminosity Experiments at the LHC". DRDC/P56, CERN/DRDC 94-21, (May 1994).

[4] St. Gobain/Norton Diamond Film, Goddard Road, Northboro, MA 01532, USA.

De Beers Industrial Diamond Division Ltd., Charters, Sunninghill, Ascot, Berkshire, SL5 9PX England.

[5] S. Zhao, "Characterization of the Electrical Properties of Polycrystalline Diamond Films", Ph.D. Dissertation, Ohio State University (1994).

[6] W. Adam *et al.* (RD42-Collaboration). "Development of Diamond Tracking Detectors for High Luminosity Experiments at the LHC". CERN/LHCC 97-3, Status Report/RD42, CERN (Jan.1997).

[7] L.S. Pan *et al.*, "Particle- and Photo-induced Currents in Type II Diamond". J. Appl. Phys. 74 (1993) 1086

[8] W. Adam *et al.* (RD42-Collaboration). "Development of CVD Diamond Radiation Detectors". 5^{th} Int. Symposium on Diamond Materials, Paris (1997).

[9] M.A. Plano *et al.*, "Thickness Dependence of the Electrical Characteristics of Chemical Vapour Deposited Diamond Film". Appl. Phys. Lett. 62 (1994) 193

[10] C. Bauer *et al.* (RD42-Collaboration). "Radiation Hardness Studies of CVD Diamond Detectors". Nucl. Instr. and Meth. A 367 (1995) 207-211

[11] W. Adam *et al.* (RD42-Collaboration). "Development of Diamond Tracking Detectors for High Luminosity Experiments at the LHC". CERN/LHCC 98-20, Status Report/RD42, (12 June 1998).

[12] D. Meier *et al.* (RD42-Collaboration). "Proton Irradiation of CVD Diamond Detectors for High Luminosity Experiments at the LHC". 2nd Int. Conf. on Radiation Effects on Semiconductor Materials, Detectors and Devices, Florence 1998. CERN-EP/98-79, to be published in Nucl. Instr. and Meth. A.

[13] M. Edwards and D.R. Perry, "The Radiation Hardness Test Facility". RAL Report RAL-90-065 (1990) 21

[14] IDE AS, Integrated Detectors & Electronics. "The VA Circuits". Catalogue, 95/96. Veritasveien 9, N-1322 Hovik, Norway.

[15] O. Toker *et al.*, "VIKING, a CMOS Low Noise Monolithic 128 Channel Frontend for Si-Strip Detector Readout". Nucl. Instr. and Meth. A 340 (1994) 572-579

[16] F. Anghinolfi *et al.*, "SCTA - A Radiation Hard BiCMOS Analogue Readout ASIC for the ATLAS Semiconductor Tracker". IEEE Trans. Nucl. Sci., 44 (1997) 298-302

[17] Boeing Defense and Space Group, Anaheim, CA , USA.

[18] J. Conway *et al.*, "The Status of Diamond Detectors and a Proposal for R&D for CDF Beyond Run II". CDF/DOC/TRACKING/PUBLIC/4233, July 10, 1997